Inorg. Chem. **2005**, *44*, 5293–5303

On the Lamellar Compounds $CuBiP_2Se_6$, $AgBiP_2Se_6$ and $AgBiP_2S_6$. Antiferroelectric Phase Transitions Due to Cooperative Cu^+ and Bi^{3+} Ion Motion

Matthew A. Gave,[†] Daniel Bilc,[‡] S. D. Mahanti,[‡] Jean D. Breshears,[†] and Mercouri G. Kanatzidis*[,†]

Department of Chemistry and Department of Physics and Astronomy, Michigan State University, East Lansing, Michigan 48824

Received March 8, 2005

$CuBiP_2Se_6$, $AgBiP_2Se_6$, and $AgBiP_2S_6$ were prepared from the corresponding elements. $CuBiP_2Se_6$ and $AgBiP_2Se_6$ crystallize in the space group $R\bar{3}$ with $a = 6.5532(16)$ Å and $c = 39.762(13)$ Å for $CuBiP_2Se_6$ and $a = 6.6524(13)$ Å and $c = 39.615(15)$ Å for $AgBiP_2Se_6$. $AgBiP_2S_6$ crystallizes in the triclinic space group $P\bar{1}$ with $a = 6.3833(13)$ Å, $b = 7.1439(14)$ Å, $c = 9.5366(19)$ Å, $\alpha = 91.89(3)°$, $\beta = 91.45(3)°$, $\gamma = 94.05(3)°$. $CuBiP_2Se_6$ was found to exhibit a temperature-dependent antiferroelectric ordering of the Cu^+ and Bi^{3+} ions in the lattice. An intermediate and a fully ordered structure were refined at 173 and 97 K, respectively. Electronic band and total energy calculations at the DFT level clearly suggest that the antiferroelectric model is energetically favored over the paraelectric and hypothetical ferrielectric models. This phase transition can be classified as a second-order Jahn–Teller distortion. The antiferroelectric state of $CuBiP_2Se_6$ is an indirect gap semiconductor. The compounds were characterized with differential thermal analysis and solid-state UV/vis diffuse reflectance spectroscopy. Generalized implications regarding the expected ferroelectric behavior of compounds in the $CuMP_2Se_6$ system (M = trivalent metal) are discussed.

Introduction

Alkali metal selenophosphate compounds with group 15 elements such as AMP_2Se_6 (A = K, Rb, Cs, M = Sb, Bi) exhibit closely related structures with a covalently bonded anionic $[MP_2Se_6]^{1-}$ framework and alkali metals as counterions.[1] There have been several discussions in the literature regarding the influence of cation size on the structure of the anion that highlight the general tendency that, for a given stoichiometry, larger counterions favor lower dimensionality in the anions.[2−4] Alkali metal interactions with the $^1/_\infty[BiP_2Se_6]^{1-}$ framework are predominantly electrostatic in nature. In the case of $KSbP_2Se_6$, three different interconvertible forms (α, β, and amorphous) were identified.[1] The conversion from one form to another is connected to the ability of K^+ ions to move inside the structure. Given the same ionic charge of coinage metals (i.e. Cu, Ag) with those of the alkali ions, it is often useful to consider the former as pseudo-alkali ions. Therefore, in general it becomes interesting to explore the relationship of alkali metal compounds to analogous compounds with Cu and Ag. By substituting the less electropositive Ag or Cu for an alkali metal, significant changes in the crystal and electronic structure are expected not only due to the counterion effect[4] but also due to the stronger Ag−Q and Cu−Q interactions compared with the electrostatic A−Q interactions (Q = chalcogen element). This is clearly manifested in the marked reductions in size of the energy band gap as observed for example in $A_{0.5}M_{1.75}GeQ_4$ (A = Ag, Cu, Na; M = Pb, Eu; Q = S, Se).[5] Exploring coinage metal/alkali metal interactions could allow the manipulation of structures and the possible tuning of the optical and electronic properties.

In this context, we targeted for study $CuBiP_2Se_6$, $AgBiP_2Se_6$, and $AgBiP_2S_6$. The first two phases have been

* Corresponding author. E-mail: kanatzid@cem.msu.edu.
[†] Department of Chemistry.
[‡] Department of Physics and Astronomy.

(1) (a) Breshears, J. D.; Kanatzidis, M. G. *J. Am. Chem. Soc.* **2000**, *122*, 7839−7840. (b) Breshears, J. D.; Kanatzidis, M. G. Unpublished results. (c) McCarthy, T. J. Ph.D. Thesis, Michigan State University, East Lansing, MI, 1994.
(2) Chondroudis, K.; Hanko, J.; Kanatzidis, M. G. *Inorg. Chem.* **1997**, *36*, 2623−2632.
(3) Chondroudis, K.; Kanatzidis, M. G. *J. Solid State Chem.* **1998**, *138*, 321−328.
(4) Kanatzidis, M. G. *Phosphorus Sulfur and Silicon* **1994**, *93*−*94*, 159−172.
(5) Iyer, R. G.; Aitken, J. A.; Kanatzidis, M. G. *Solid State Sci.* **2004**, *6*, 451−459.

10.1021/ic050357+ CCC: $30.25
Published on Web 06/30/2005

described briefly and were claimed to possess photoconductive properties; however, their structural characterization has not been reported.[6] Furthermore, Cu and Ag in these types of compounds can become mobile and cause the materials to undergo interesting phase transitions. This is observed in the related layered compounds of $CuInP_2S_6$, $CuInP_2Se_6$, $AgAlP_2Se_6$ $CuCrP_2Se_6$, and $CuVP_2S_6$. These compounds show interesting physical properties such as ferri- and ferroelectricity with high spontaneous polarization,[7−9] as well as strong second harmonic generation[10] and photoelectric response.[11]

Here we describe $CuBiP_2Se_6$, $AgBiP_2Se_6$, and $AgBiP_2S_6$, which represent the coinage metal analogues of the $ABiP_2Q_6$ group. The stronger and more covalent interactions of Cu^+ and Ag^+ ions with the framework $[BiP_2Se_6]^{1-}$ coupled with their small size results in a distinctly different lamellar motif from those of the alkaline metal counterparts. Interestingly, $CuBiP_2Se_6$ exhibits temperature-induced antiferroelectric phase transitions associated with the motion of Cu^+ ions in the structure, whereas $AgBiP_2Se_6$ is already at this antiferroelectric state at room temperature.

Experimental Section

Reagents. Chemicals were used as obtained, unless otherwise noted: bismuth chunks (99.999%, Tellurex Inc.), selenium shot (99.999%, Tellurex Inc.), sulfur (sublimed flowers, Alfa Aesar), phosphorus (amorphous red, MCB Reagents), electrolytic copper dust (Fisher Scientific), and silver powder (prepared as below). Selenium and bismuth were ground in an agate mortar and pestle to ca. 100 mesh.

Synthesis. Preparation of Silver Powder. Silver powder was prepared by cutting a silver coin (31 g) into centimeter-sized pieces and dissolving them in 200 mL concentrated nitric acid by stirring overnight. The solution was then neutralized by addition of ammonium hydroxide. Finely divided silver particles were obtained after addition of 10 g of sodium borohydride to the solution and were isolated by filtration, washed with water, and dried in a 100 °C oven.

$CuBiP_2Se_6$. A mixture of Cu (0.1580 g. 2.5 mmol), Bi (0.5179 g. 2.5 mmol), P (0.1549 g. 5.0 mmol), and Se (1.1816 g. 15.0 mmol) was loaded into a fused silica tube and flame-sealed at a reduced pressure of $<10^{-4}$ mbar. The mixture was heated to 700 °C over 12 h and held for 12 h, followed by cooling to 50 °C at a rate of −15 °C/h. An inhomogeneous gray metallic ingot (approximately 80% product, 20% Bi_2Se_3/Cu_3PSe_4) was isolated that fractured into graphite-like layers composed of air-stable black plates. Microprobe analysis of single crystals gave an average composition of $Cu_{1.0}Bi_{1.0}P_{2.2}Se_{5.8}$.

$AgBiP_2Se_6$. A mixture of Ag (0.2532 g., 2.35 mmol), Bi (0.4918 g., 2.35 mmol), P (0.1466 g. 4.7 mmol), and Se (1.1205 g. 14.2 mmol) was loaded into a fused silica tube that was flame-sealed at a reduced pressure of $<10^{-4}$ mbar and was heated with the same profile as above. An inhomogeneous gray metallic ingot (approximately 80% product, 20% $AgBiSe_2$) was isolated that fractured into graphite-like layers composed of air-stable black plates. Microprobe analysis of single crystals gave an average composition of $Ag_{1.1}Bi_{1.0}P_{2.0}Se_{5.9}$.

$AgBiP_2S_6$. A mixture of Ag (0.1803 g., 1.7 mmol), Bi (0.3463 g., 1.7 mmol), P (0.1565 g. 5.1 mmol), and S (0.3203 g. 10.0 mmol) was loaded into a fused silica tube and flame-sealed at a reduced pressure of $<10^{-4}$ mbar. The mixture was heated to 850 °C over 12 h and kept there for 24 h, followed by cooling to 50 °C at a rate of −15 °C/h. A homogeneous gray metallic-like ingot was obtained, but it was coated with an amorphous red phosphorus powder. Upon fracturing, the ingot cleaved in a graphite-like manner to form black plates. Microprobe analysis gave an average composition of $Ag_{1.0}Bi_{1.0}P_{2.1}S_{6.0}$. The phase was pure by powder X-ray diffraction, although it is likely that some amorphous elemental phosphorus was present.

Powder X-ray Diffraction. All samples were assessed for phase purity using powder X-ray diffraction. Powder patterns were obtained using an Inel CPS 120 powder X-ray diffractometer with monochromatized Cu Kα radiation (λ = 1.540 598 Å) operating at 40 kV and 20 mA equipped with a position-sensitive detector with a 2θ range of 0−120° and calibrated with a $Na_2Ca_3Al_{12}F_{14}$ standard.[12]

Single-Crystal X-ray Diffraction. Intensity data for single crystals of $CuBiP_2Se_6$ and $AgBiP_2Se_6$ were collected on a Bruker SMART platform CCD diffractometer using Mo Kα radiation operating at 40 kV and 40 mA. Individual frames were collected with a 10 s exposure time and a 0.3° ω rotation. The SMART software was used for data collection, and SAINT software was used for data extraction and reduction. An analytical absorption correction to the data was performed, and direct methods were used to solve and refine the structures with the SHELXTL software package.

Intensity data for $AgBiP_2S_6$ was collected on a Stoe IPDS II diffractometer with Mo Kα radiation operating at 50 kV and 40 mA with a 34 cm image plate. Individual frames were collected with a 60 s exposure time and a 0.5° ω rotation. The X-SHAPE and X-RED software packages were used for data extraction and reduction and to apply an analytical absorption correction. The SHELXTL software package was used to solve and refine the structure. The parameters for data collection and the details of the structural refinement can be found in Table 1. Fractional atomic coordinates and displacement parameters for each structure are given in Tables 2−6. In all cases the atoms were refined to full occupancy.

Electron Microscopy. A JEOL JSM-35C scanning electron microscope equipped with a Tracor Northern energy dispersive spectroscopy detector was used for quantitative microprobe analysis. Data were collected using an accelerating voltage of 25 kV and a collection time of 60s.

Differential Thermal Analysis. Differential thermal analyses were performed with a Shimadzu DTA-50 thermal analyzer. A portion of the ingot obtained from the reaction weighing ca. 25 mg was finely ground and sealed in a quartz ampule under reduced pressure. An equivalent mass of alumina was sealed in an identical ampule to serve as a reference. The samples were heated to 800 °C at a rate of 10 °C/min, cooled to 150 °C at a rate of 10 °C/min, reheated to 800 °C at a rate of 10 °C/min, and then cooled to room temperature at a rate of 10 °C/min.

(6) Galdamez, A.; Manriquez, V.; Kasaneva, J.; Avila, R. E. *Mater. Res. Bull.* **2003**, *38*, 1063−1072.
(7) Simon, A.; Ravez, J.; Maisonneuve, V.; Payen, C.; Cajipe, V. B. *Chem. Mater.* **1994**, *6*, 1575−1580.
(8) Vysochanskii,Y. *Ferroelectrics* **1998**, *218*, 629−636.
(9) Ysochanskii,Y.; Molnar, A.; Gurzan, M.; Cajipe, V.; Bourdon, X. *Solid State Commun.* **2000**, *115*, 13−17.
(10) Misuryaev, T. V.; Murzina, T. V.; Aktsipetrov, O. A.; Sherstyuk, N. E.; Cajipe, V. B.; Bourdon, X. *Solid State Commun.* **2000**, *115*, 605−608.
(11) Pfeiff, R.; Kniep, R. *J. Alloys Compd.* **1992**, *186*, 111−133.
(12) Evain, M.; Deniard, P.; Jouanneaux, A.; Brec, R. J. *Appl. Crystallogr.* **1993**, *26*, 563−569.

Table 1. Crystallographic Data and Experimental and Refinement Details for the Reported Phases

	$CuBiP_2Se_6$	$CuBiP_2Se_6$	$CuBiP_2Se_6$	$AgBiP_2Se_6$	$AgBiP_2S_6$
temp, K	298	173	97	298	298
crystal system	trigonal	rhombohedral	rhombohedral	rhombohedral	triclinic
space group	$P\bar{3}1c$	$R\bar{3}$	$R\bar{3}$	$R\bar{3}$	$P\bar{1}$
λ, Å (Mo Kα)	0.071 073	0.071 073	0.071 073	0.071 073	0.071 073
a, Å	6.5410(9)	6.5591(10)	6.5532(16)	6.6524(13)	6.3833(13)
b, Å	6.5410(9)	6.5591(10)	6.5532(16)	6.6524(13)	7.1439(14)
c, Å	13.263(3)	79.385(18)	39.762(13)	39.615(15)	9.5366(19)
α, deg	90	90	90	90	91.89(3)
β, deg	90	90	90	90	91.45(3)
γ, deg	120	120	120	120	94.05(3)
Z	2	12	6	6	2
crystal dimensions, mm	0.18 × 0.18 × 0.04	0.16 × 0.15 × 0.02	0.16 × 0.15 × 0.02	0.24 × 0.22 × 0.07	0.31 × 0.18 × 0.09
D_{calc}, g/cm^3	5.462	5.445	5.445	5.595	4.377
μ, mm^{-1}	42.513	42.381	42.383	41.116	24.26
R_{int}, %	5.8	6.5	5.8	5.8	3.2
total reflections/independent	1678/220	8151/1626	2947/799	3000/498	4155/2136
final R/R_w, %[a]	5.5/13.9	9.1/21.2	5.0/11.7	4.5/9.9	4.2/9.2

[a] $R = \sum(|F_o| - |F_c|)/\sum|F_o|$. $R_w = [\sum w(|F_o| - |F_c|)^2/\sum w|F_o|^2]^{1/2}$.

Table 2. Fractional Atomic Coordinates and U_{eq} Values for $CuBiP_2Se_6$ at 298 K with Standard Deviations in Parenthesis

atom	x	y	z	U_{eq}[a]	symmetry
Bi	1.3333	0.6667	0.7500	15(1)	2d
Se	1.3322(3)	0.3031(3)	0.6180(1)	20(1)	12i
Cu	1.0000	1.0000	0.7500	186(8)	2a
P	1.6667	0.3333	0.6652(6)	10(2)	4f

[a] $U_{eq} = (\sum_i\sum_j U_{ij}a_i^*a_j^*a_ia_j)/3 \times 1000$.

Table 3. Fractional Atomic Coordinates and U_{eq} Values for $CuBiP_2Se_6$ at 173 K with standard deviations in parentheses

atom	x	y	z	U_{eq}[a]	symmetry
Bi(1)	0.6667	0.3333	0.0412(1)	17(1)	6c
Bi(2)	0.3333	−0.3333	0.1222(1)	15(1)	6c
Se(1)	0.7200(4)	0.0410(4)	0.1031(1)	19(1)	18f
Se(2)	1.0312(4)	0.7015(4)	0.0196(1)	22(1)	18f
Se(3)	0.3503(4)	0.0099(4)	0.1473(1)	16(1)	18f
Se(4)	1.0271(4)	0.3363(4)	0.0638(1)	20(1)	18f
P(1)	1.3333	0.6667	0.0558(1)	15(2)	6c
P(2)	0.6667	0.3333	0.1385(1)	11(2)	6c
P(3)	0.6667	0.3333	0.1104(1)	13(2)	6c
P(4)	1.3333	0.6667	0.0275(1)	14(2)	6c
Cu(1)	2.0000	1.0000	0.1369(2)	91(4)	6c
Cu(2)	0.0000	0.0000	0.0430(3)	178(9)	6c

[a] $U_{eq} = (\sum_i\sum_j U_{ij}a_i^*a_j^*a_ia_j)/3 \times 1000$.

Table 4. Fractional Atomic Coordinates and U_{eq} Values for $CuBiP_2Se_6$ at 97 K with Standard Deviations in Parenthesis

atom	x	y	z	U_{eq}[a]	symmetry
Bi	0.0000	0.0000	0.0907(1)	10(1)	6c
Se(1)	0.3761(2)	0.3877(2)	0.1273(1)	12(1)	18f
Se(2)	0.3389(2)	1.0230(2)	0.0386(1)	9(1)	18f
Cu(1)	0.3333	0.6667	0.0535(1)	13(1)	6c
Cu(2)	0.3333	0.6667	0.0761(13)	47(9)	6c
P(1)	0.6667	0.3333	0.1128(1)	9(1)	6c
P(2)	0.6667	1.3333	0.0561(1)	7(1)	6c

[a] $U_{eq} = (\sum_i\sum_j U_{ij}a_i^*a_j^*a_ia_j)/3 \times 1000$.

Solid State UV/Vis Spectroscopy. Optical band gaps were determined using Kubelka−Munk theory[13] on data collected by diffuse reflectance UV/vis spectroscopy on finely ground sample portions of the ingot at room temperature. A background was collected before each scan using $BaSO_4$. A spectrum was collected for the region of 200−2500 nm with a Shimadzu UV-3101 PC double-beam, double-monochromator spectrophotometer.

Table 5. Fractional Atomic Coordinates and U_{eq} Values for $AgBiP_2Se_6$ at 298 K with Standard Deviations in Parenthesis

atom	x	y	z	U_{eq}[a]	symmetry
Bi	0.0000	0.0000	0.0880(1)	23(1)	6c
Se(1)	0.3749(2)	0.3761(2)	0.1278(1)	26(1)	18f
Se(2)	0.3431(2)	0.0328(2)	0.0379(1)	24(1)	18f
P(1)	0.6667	0.3333	0.0555(2)	18(1)	6c
P(2)	0.6667	0.3333	0.1123(2)	18(1)	6c
Ag(1)	0.3333	-0.3333	0.0723(1)	64(1)	6c

[a] $U_{eq} = (\sum_i\sum_j U_{ij}a_i^*a_j^*a_ia_j)/3 \times 1000$.

Table 6. Fractional Atomic Coordinates and U_{eq} Values for $AgBiP_2S_6$ at 298 K with Standard Deviations in Parenthesis

atom	x	y	z	U_{eq}[a]	symmetry
Bi	0.4603(1)	0.6376(1)	0.2328(1)	23(1)	2i
Ag	0.0574(2)	1.0430(2)	0.2902(2)	58(1)	2i
P(1)	0.5603(3)	1.1182(3)	0.4357(2)	12(1)	2i
P(2)	-0.0600(3)	0.6088(3)	0.0705(2)	11(1)	2i
S(1)	0.1741(3)	0.8195(3)	0.0764(2)	14(1)	2i
S(2)	0.6533(3)	0.9989(3)	0.2518(2)	15(1)	2i
S(3)	0.3174(3)	0.3013(3)	0.0297(2)	14(1)	2i
S(4)	0.3232(4)	1.2867(3)	0.4163(3)	21(1)	2i
S(5)	0.8793(4)	0.4899(3)	0.2526(2)	16(1)	2i
S(6)	0.1944(3)	0.7559(3)	0.4522(2)	17(1)	2i

[a] $U_{eq} = (\sum_i\sum_j U_{ij}a_i^*a_j^*a_ia_j)/3 \times 1000$.

Method of Electronic Structure Calculations. Electronic structure calculations were performed using the self-consistent full-potential linearized augmented plane wave method (LAPW)[14] within density functional theory (DFT)[15] and the generalized gradient approximation (GGA) of Perdew, Burke and Ernzerhof[16] for the exchange and correlation potential. The values of the atomic radii were taken to be 1.8 au for P atoms, 2.2 au for Se and Cu atoms, and 2.6 au for Bi atoms, where au is the atomic unit (0.529 Å). Convergence of the self-consistent iterations was performed for 20K points inside the irreducible Brillouin zone to within 0.0001 Ry with a cutoff of −6.0 Ry between the valence and the core states.

(13) (a) Wendlandt, W. W.; Hecht, H. G. *Reflectance Spectroscopy*; Interscience Publishers: New York, 1966. (b) Kotum, G. *Reflectance Spectroscopy*; Springer-Verlag: New York, 1969. (c) Tandon, S. P.; Gupta, J. P. *Phys. Status Solidi* **1970**, *38*, 363−367.

(14) Singh, D. *Planewaves, Pseudopotentials, and the LAPW Method*; Kluwer Academic: Boston, MA, 1994.

(15) (a) Hohenberg, P.; Kohn, W. *Phys. Rev.* **1964**, *136*, B864−B871. (b) Kohn, W.; Sham, L. *Phys. Rev.* **1965**, *140*, A1133-A1138.

(16) Perdew, J. P.; Burke, K.; Ernzerhof, M. *Phys. Rev. Lett.* **1996**, *77*, 3865−3868.

Scalar relativistic corrections were included, and a spin−orbit interaction was incorporated using a second variational procedure.[17] The calculations were performed using the program WIEN2K.[18]

Results and Discussion

$CuBiP_2Se_6$ and $AgBiP_2Se_6$ formed as black crystal plates. It was not possible to obtain pure compounds, as the former always contained Bi_2Se_3 and Cu_3PSe_4 and the latter $AgBiSe_2$ as minor phases. The bulk samples were gray metallic in appearance and broke into graphite-like layers upon cracking. In our hands a procedure given for these compounds in an earlier report could not be repeated.[6]

Neither the use of P_2Se_5 nor RbCl/LiCl flux was successful in producing pure phases of the desired compounds. In each attempt, as much as a 20% Bi_2Se_3/Cu_3PSe_4 or $AgBiSe_2$ impurity was found by powder X-ray diffraction. Attempts to prepare $CuBiP_2Se_6$ and $AgBiP_2Se_6$ by quenching stoichiometric melts to room temperature or in ice water were not successful in producing the desired product as a single phase and resulted only in known binary/ternary compounds. The persistent impurities are likely the result of their extreme stability.

$CuBiP_2Se_6$ and $AgBiP_2Se_6$ are semiconductors with a room-temperature energy gap (E_g) of 1.2 and 1.4 eV respectively (Figure 1A,B). Bi_2Se_3 has a band gap of 0.35 eV and is likely the cause of the high residual absorbance below the band gap. The other impurity phase, Cu_3PSe_4, has a band gap of 1.3 eV, and therefore, the absorption edge is nearly collinear with the absorption edge of $CuBiP_2Se_6$. $AgBiSe_2$ is an impurity in $AgBiP_2Se_6$ and has a band gap of 0.5 eV, which can be seen at lower energy than the absorption edge of the $AgBiP_2Se_6$. The band gaps of the dominant phases are in a range that is considered optimum for best matching the solar energy spectrum with respect to absorption. The suitable energy gap and high crystal symmetry could result in stable photoexcited carriers with high mobility. Preliminary reports suggest that these materials can generate photoexcited carriers.[6] Therefore, these systems could be attractive for investigations as possible solar energy materials. The band gaps of the related $KBiP_2Se_6$ phases are somewhat larger than those reported here at 1.6 eV for the α-phase and 1.3 eV for the *β*-phase.[1]

DTA analysis of sample portions of the ingot containing $CuBiP_2Se_6$ and $AgBiP_2Se_6$ melt incongruently at 475 and 480 °C, respectively. A broad endothermic region in both cases suggested that the title phases form a eutectic mixture with the corresponding impurity phases. Powder X-ray diffraction of the sample portion after two heating cycles indicated that the title compounds were obtained in approximately the same yield and were accompanied by the same impurities.

The synthesis of $AgBiP_2S_6$ could only be accomplished in the presence of an additional equivalent of phosphorus. In each attempt with the stoichiometric ratio, phosphorus was oxidized to the 5+ state and produced ternary compounds containing $[PS_4]^{3-}$ units (e.g. Ag_7PS_6, Ag_3PS_4). Apparently, the extra equivalent of phosphorus helps to achieve the P^{4+}-containing $[P_2S_6]^{4-}$ anions from which $AgBiP_2S_6$ could form. The material was found to melt at 590 °C by DTA. A parallel attempt to produce $CuBiP_2S_6$ using extra phosphorus in the synthesis was not successful, instead producing the very stable phases Cu_3PS_4 and $BiPS_4$. A band gap of 1.7 eV was determined spectroscopically for $AgBiP_2S_6$ (Figure 1C).

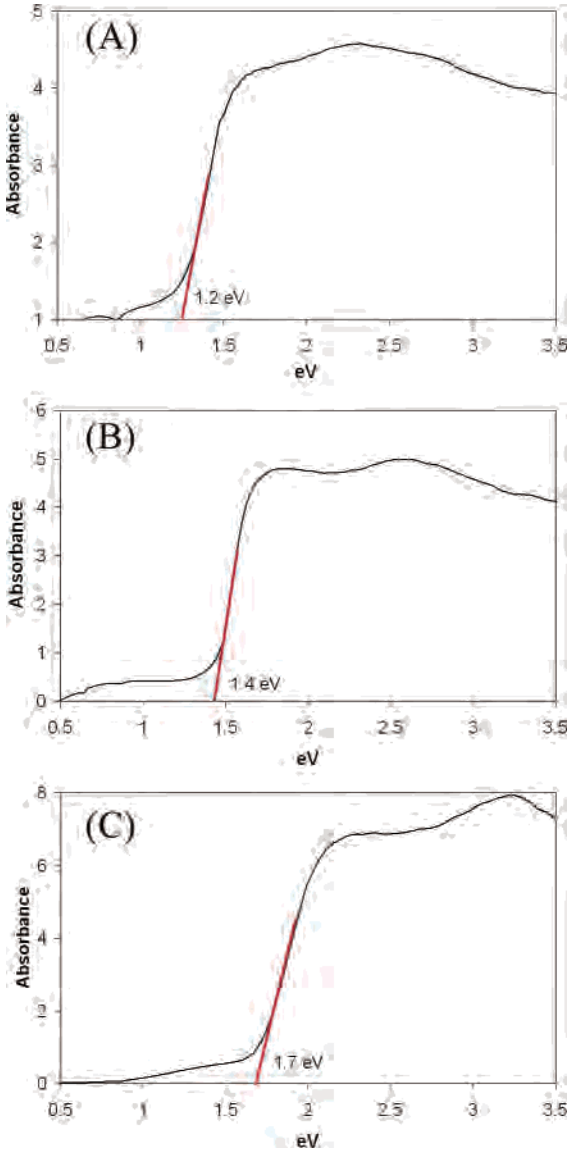

Figure 1. The optical absorption spectra of (A) $CuBiP_2Se_6$, (B) $AgBiP_2Se_6$, and (C) $AgBiP_2S_6$. The high residual absorbance below the band gap in spectrum A is likely the result of a Bi_2Se_3 impurity and that in spectrum B the result of $AgBiSe_2$.

Structure Description. Not surprisingly, the phases reported here do not adopt the same structure as their alkali-containing analogues $KBiP_2Se_6$ and $RbBiP_2Se_6$, which feature pseudo-one-dimensional structures. Because of the smaller size of Cu^+ and Ag^+ ions, the $[BiP_2Se_6]^{1-}$ anion favors a two-dimensional structure that interacts strongly with the coinage metals and "traps" them inside it. This structure is similar to other Cu and Ag selenophosphates containing group 13 metals (e.g. Al^{3+}, In^{3+}).

$CuBiP_2Se_6$ and $AgBiP_2Se_6$. These compounds have the lamellar $Fe_2P_2Se_6$ structure type. This structure is a modifica-

(17) Koelling, D. D.; Harmon, B. *J. Phys. C* **1977**, *10*, 3107

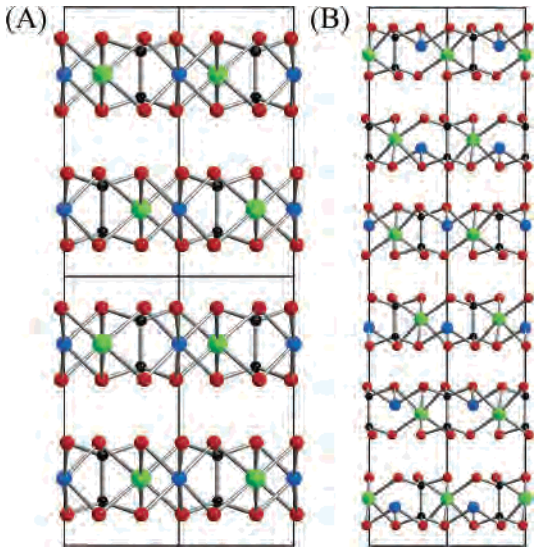

Figure 2. The layered structures of (A) $CuBiP_2Se_6$ and (B) $AgBiP_2Se_6$ (room temperature) view down the [110] direction. Blue atoms are Cu(Ag), green atoms are Bi, red atoms are Se, and black are atoms P.

tion of the CdI_2 structure where $^1/_3$ of the metal sites are replaced with a $[P_2Se_6]^{4-}$ anion with the P−P bond axis along the layer normal. Each layer has the thickness of one $[P_2Se_6]^{4-}$ unit (Figure 2), and the structures contain well-defined van der Waals gaps. Because of differences in the stacking sequence (i.e. positions on the slabs relative to each other), the two compounds are not isomorphous and, at room temperature, adopt hexagonal and rhombohedral space groups respectively (Table 1).

The structures are closely related to those of $CuCrP_2Se_6$ and $CuInP_2Se_6$ with the same $[P_2Se_6]^{4-}$ anion lattice bridged by the metal cations. This $Fe_2P_2Se_6$ slab motif is generally adopted by compounds with transition M^{2+} metal ions or a combination of M^+/M^{3+} ions (e.g. Cu/Al, Ag/In, Cu/Cr) that have no valence electrons (i.e. have a $d^ns^0p^0$ configuration). When transition M^{2+} metals are replaced with main group elements, which formally possess ns^2 configuration (e.g. Pb^{2+}, Sn^{2+}), the lamellar $M_2P_2Se_6$ structure type changes to a three-dimensional one.[19] Therefore, it is interesting that in $CuBiP_2Se_6$ and $AgBiP_2Se_6$, where an intermediate situation exists, i.e., half the metal sites are Bi^{3+} ($6s^2$), the lamellar $Fe_2P_2Se_6$ motif is preserved.

The $[P_2Se_6]^{4-}$ anions in the room-temperature structure of $CuBiP_2Se_6$ and $AgBiP_2Se_6$ are bridged by an ordered arrangement of alternating coinage metal and bismuth metal centers. Each anion has three coinage metal ions and three bismuth ions as its nearest metal neighbors (Figure 3). The Cu^+ ions in $CuBiP_2Se_6$ have an octahedral coordination environment of Se atoms (Figure 4A). This is unusually high

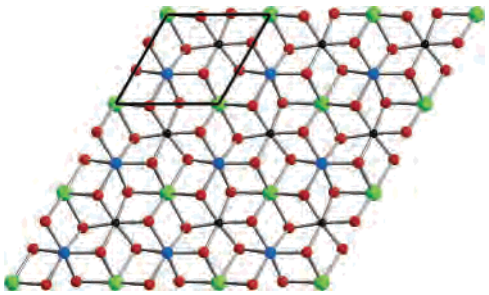

Figure 3. View of a single $CuBiP_2Se_6$ layer down the *c*-axis ([001] direction) showing the ordered arrangement of the Bi^{3+} and Cu^+ ions. The same arrangement exists in $AgBiP_2Se_6$.

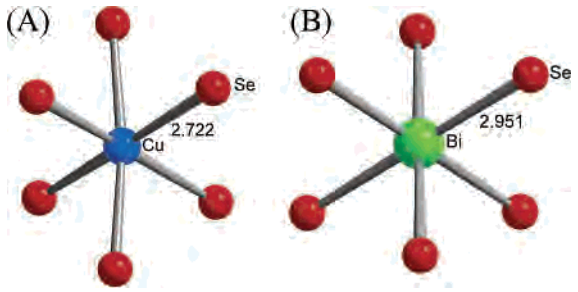

Figure 4. The immediate coordination environment of (A) Cu^+ and (B) Bi^{3+} in $CuBiP_2Se_6$ at room temperature.

for Cu, since it is well-known that, in chalcogenides, Cu prefers low coordination sites such as tetrahedral, trigonal planar, or even linear. In fact, by inspecting the results of the crystal structure refinement, there is strong evidence that the apparent high coordination environment of Cu is misleading. As suggested by the very high anisotropic thermal parameter of Cu^+ ions, $U_{11} = U_{22} = 175(11)$ and $U_{33} = 209(18)$, it is likely that this is the result of dynamic averaging due to atomic motion in an oversized cavity. This suggests that the actual position of Cu is a disordered arrangement of various off-center positions.[20] By moving off center, the Cu^+ ions can achieve a lower coordination environment.

The Bi site is nearly octahedral with Bi−Se bond lengths of 2.950(2) Å and Se−Bi−Se bond angles ranging from 88.37(6)° to 91.79(7)°. The so-called $6s^2$ lone pair on Bi is thus not stereochemically expressed (Figure 4B). The P−Se distance is 2.187(3) Å and the P−P distance is 2.251(16) Å. In contrast to the Cu analogue, Ag^+ ion disorder is not evident in $AgBiP_2Se_6$, where these ions are already situated in an off-center position inside a Se-based octahedron.

The positions of Ag^+ ions in $AgBiP_2Se_6$ are distorted from an octahedral environment by an elongation of three of the Ag−Se bonds, thus shifting the Ag^+ ions along the *c*-axis away from the center of the layer by 0.4 Å (Figure 5A). All Ag^+ ions are ordered at room temperature, in contrast to the disorder observed in $CuBiP_2Se_6$, described above. The Bi site is a slightly distorted octahedron with Bi−Se bond lengths from 2.9487(15) to 2.9550(15) Å and Se−Bi−Se angles ranging from 79.70(5)° to 95.35(4)° (Figure 5B). The Bi^{3+} ions are shifted only 0.2 Å off the center of the

(18) Blaha, P.; Schwarz, K.; Madsen, G.; Kvasnicka, D.; Luitz, J. *WIEN2K, An Augmented Plane Wave + Local Orbitals Program for Calculating Crystal Properties*; Karlheinz Schwarz Technical University: Wien, Vienna, 2001.

(19) (a) Becker, R.; Brockner, W.; Schaefer, H. *Z. Naturforch. Pt. A.* **1984**, *39*, 357−361. (b) Israel R.; Eijt, S. W. H.; de Gelder, R.; Smits, J. M. M.; Beurskens, P. T.; Rasing, T.; van Kempen, H.; Maior, M. M.; Motrija, S. F. *Z. Kristallogr.* **1998**, *213*, 34−41. (c) Lee, S. *J. Am. Chem. Soc.* **1988**, *110*, 8000−8006.

(20) A higher order anharmonic refinement using the Jana2000 software was not successful in reducing the copper thermal parameter.

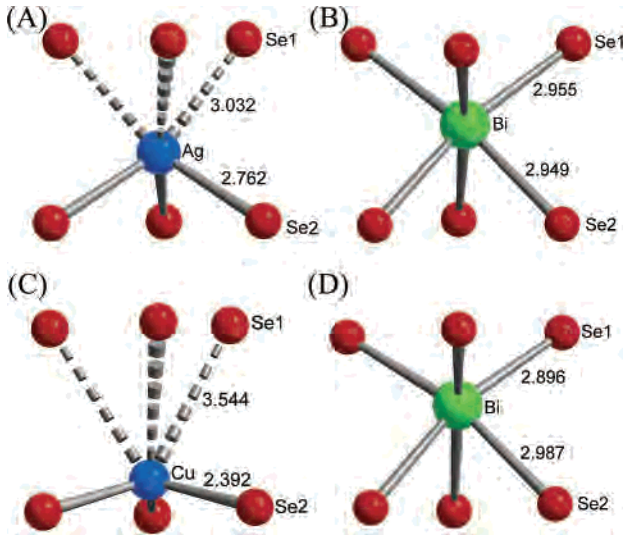

Figure 5. The immediate coordination environments of (A) Ag^+ and (B) Bi^{3+} atoms in $AgBiP_2Se_6$ at 298 K; (C) Cu and (D) Bi atoms in $CuBiP_2Se_6$ at 97 K.

octahedron in the opposite direction along the layer normal of the Ag^+ ions. Again, the $6s^2$ lone pair of Bi does not seem to be stereochemically expressed. The Ag−Se bond lengths are 2.762(2) Å, with presumably weak bonding to the other side of the Se cage 3.032(3) Å away. The P−Se distances range from 2.186(2) to 2.193(2) Å, and the P−P distance is 2.251(9) Å.

Temperature-Induced Cu^+ Sublattice Ordering. The oversized cavity of the Cu^+ ions in $CuBiP_2Se_6$ and the possible dynamic disorder in these cavities prompted us to investigate the possibility of ordering at lower temperatures. For $CuBiP_2Se_6$ we refined the structure at three different temperatures (97, 173, and 298 K) and indeed discovered ordering in the form of two well-defined antiferroelectric transitions as the Cu^+ ions move and settle off-center of the octahedral sites (Figure 6).

The antiferroelectric order of Ag^+ ions observed in $AgBiP_2Se_6$ at room temperature is achieved in $CuBiP_2Se_6$ as the sample is cooled to <97 K. On its way to the fully ordered state the system passes through a series of intermediate structures with some slabs being fully ordered and others disordered. The low-temperature structure (97 K) has six layers per unit cell (Figures 6C, 2B). Adjacent layers are shifted with respect to each other by one-third along the *a*- or *b*-axes.

As the temperature is lowered from 298 to 173 K, a new unit cell with a 6-fold superstructure along the *c*-axis was observed. The refinement of the structure at 173 K suggested an intermediate structure in the phase transition, as seen in Figure 6B. The Cu^+ ions in six of the twelve "$CuBiP_2Se_6$" layers move in a direction parallel to the *c*-axis and toward the triangular face of the octahedral Se-cage. This motion is such that Cu^+ ions in adjacent slabs move in opposite directions and toward the same van der Waals gap. This results in an antiferroelectric arrangement. In the remaining layers the Cu^+ ions are still disordered within the selenium cage and exhibit a very high thermal displacement parameter.

At 97 K the transition of the Cu^+ ions to a fully ordered state is nearly complete, with about 85% of the Cu^+ ions in a well-defined off-center position: 1.16 Å away from the center of the octahedron along the 3-fold axis. The remaining 15% of Cu^+ ions are still disordered within the layer as before but have been omitted for clarity (Figure 6C). Presumably, at a lower temperature, all of the Cu^+ ions would be ordered.[21]

The Cu^+ ion motion creates a dipole moment inside the $CuBiP_2Se_6$ slab and a new trigonal pyramidal coordination environment with Cu−Se distances of 2.3917(17) Å (Figure 5C). The long Cu···Se distances to the opposite side are 3.544(1) Å. At the same time, however, the Bi^{3+} ions within the same layer displace in a similar manner but in the opposite direction of the Cu^+ ions (Figure 5D). The displacement of Bi^{3+} ions is 0.31 Å from the octahedral center and it creates an almost equal but opposite dipole moment. It is interesting that these ions that bear thrice the charge of the Cu^+ ions move only one-third the distance. This gives rise to a formal antiferroelectric arrangement inside the slab and results in an intraslab dipole moment cancellation.

Other examples where temperature-dependent Cu atom ordering has been reported include $CuInP_2S_6$ (315 K),[7] $CuCrP_2Se_6$ (40 K), $CuInP_2Se_6$ (240 K),[22] and $CuVP_2Se_6$ (20 K).[23] In $CuInP_2Se_6$, the motion of Cu^+ and In^{3+} ions is such that a net dipole moment remains and a ferroelectric phenomenon is produced. The Cu^+ ions in $CuInP_2Se_6$ move 1.18 Å off center in the same direction along the slab-normal, whereas the In^{3+} ions do not move appreciably. This causes a net dipole moment in the slab that then induces the corresponding moments in adjacent slabs to align ferroelectrically.

At 1.16 Å, the magnitude of the displacement of the Cu^+ ions at room temperature in $CuBiP_2Se_6$ is comparable to that in $CuInP_2Se_6$. This large Cu^+ ionic displacement in $CuBiP_2Se_6$ and in $CuBiP_2Se_6$ may be attributed to the degree of covalency between the Cu and Se atoms. The ordering at low temperatures is likely the result of a second-order Jahn−Teller coupling involving the copper d-orbitals and the selenium orbitals.[22]

A conversion to a disordered arrangement of coinage metal was not evident in either Ag analogue. It is possible, however, that above room-temperature a disordered paraelectric phase exists. The reasons for the differences in behavior observed between $CuBiP_2Se_6$ (antiferroelectric) and $CuInP_2Se_6$ (ferroelectric) could be traced to the existence of the stereochemically active lone pair in Bi^{3+}. The stereochemical expression of this excess electron density on one side of the Bi^{3+} atom is the driving force for shifting it off the octahedron center, a counteraction that cancels the Cu-induced dipole moment. The inability of In^{3+} to behave similarly obviates the need for a comparable shift in its

(21) The temperature of 97 K was the lowest accessible by our X-ray diffractometer.

(22) Bourdon, X.; Maisonnevue, V.; Cajipe, V. B.; Payen, C.; Fischer, J. E. *J. Alloys Compd*. **1999**, *283*, 122−127.
(23) Burr, G.; Durand, E.; Evain, M.; Brec, R. *J. Solid State Chem*. **1993**, *103*, 514−518

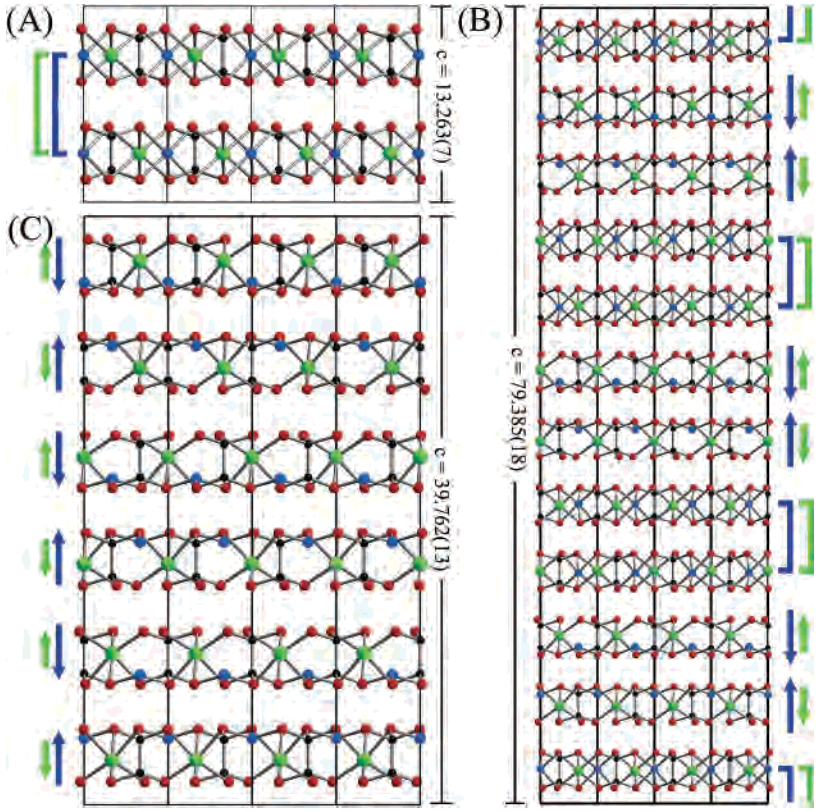

Figure 6. The (A) 298 K (B) 173 K, and (C) 97 K structures of $CuBiP_2Se_6$ viewed down the [110] direction. The direction of the displacement of the copper atoms has been indicated with an arrow. The copper atoms in the layers marked with a bracket have not yet ordered.

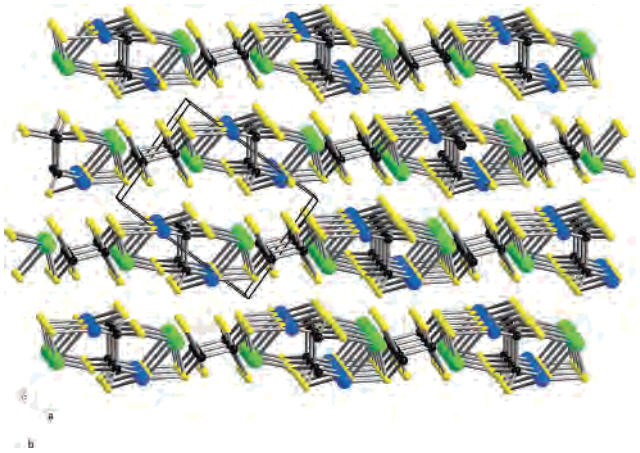

Figure 7. Structure of $AgBiP_2S_6$ viewed down the *a*-axis showing the lamellar structure.

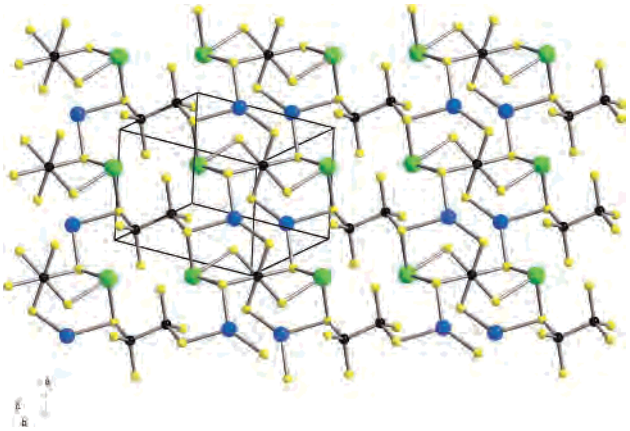

Figure 8. View of a single layer of $AgBiP_2S_6$. The P−P distance ranges from 2.212(4) to 2.225(5) Å, and the P−S distances range from 1.993(3) to 2.044(3) Å.

octahedral cage, thereby allowing the Cu-induced dipole moments to induce ferroelectric behavior in $CuInP_2Se_6$. This implies that in isostructural $CuMP_2Se_6$ systems (where M is trivalent metal) we could expect ferroelectric ordering only when M lacks a ns^2 lone pair and presents an exact size fit in the octahedral cage.

Structure of $AgBiP_2S_6$. This compound, though layered, exhibits a different structure type (Figure 7). Half of the $[P_2S_6]^{4-}$ units lie with their P−P axis normal to the layer, as in the structures described above, whereas the other half are rotated so their P−P bond axis is nearly parallel to the layer (Figure 8). The $[P_2S_6]^{4-}$ anion normal to the layer coordinates to four Ag^+ and two Bi^{3+} ions. The anions lying parallel coordinate to four Bi^{3+} and two Ag^+ ions. This is a contrast to the selenium-containing analogue that has only a perpendicular arrangement of $[P_2Se_6]^{4-}$ anions, thus forming octahedral chalcogenide cages, which in $AgBiP_2S_6$ are absent. Ag^+ ions are instead coordinated by a highly distorted tetrahedron of S atoms within the same layer and have only weak Ag−S interactions across the van der Waals gap (Figure 9A). The Bi^{3+} ions are coordinated by six S atoms with bond distances ranging from 2.752(2) to 3.106(2) Å (Figure 9B). This is a highly distorted coordination environment for Bi, and clearly there is one side of the coordination sphere that is devoid of S atoms. This suggests that the inert lone pair ($6s^2$) of Bi is strongly stereochemically expressed.

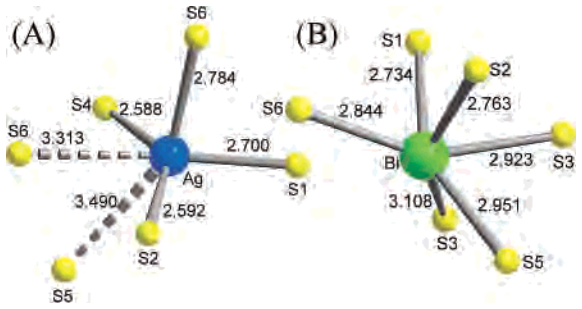

Figure 9. The immediate coordination environment of (A) Ag and (B) Bi in $AgBiP_2S_6$.

The S atoms spanning the putative lone pair (S3, S5, S6) have large S−Bi−S bond angles of 129.57(6)°−152.06(6)°. The S−Bi−S angles that do not span the lone pair have smaller bond angles: 72.86(7)°−88.77(6)°.

The inability of $AgBiP_2S_6$ to be isostructural to its Se analogue could have its origins in the large size of Bi for the available S-based octahedral cage as well as its increased tendency to stereochemically express its lone pair of electrons. Being smaller in size, the S atoms cannot fully satisfy the coordination shell of Bi, resulting in a highly distorted geometry. Differences in the observed bonding environment of Bi^{3+} ions in the sulfide- and selenide-containing structures are common, as for example in Bi_2S_3 (distorted octahedral) vis a vis Bi_2Se_3 (perfect octahedral). The large size of Bi^{3+} ions must play a dominant role to destabilize the $Fe_2P_2Se_6$ structure type given that the analogous compounds with smaller In^{3+}, $AgInP_2S_6$,[11] is in fact structurally closely related to $AgBiP_2Se_6$ and not $AgBiP_2S_6$.[24]

Electronic Structure Calculations

To understand the differences between the antiferroelectric (the structure at 97 K) and paraelectric (the structure at 298 K) phases of $CuBiP_2Se_6$, we performed electronic structure calculations for both forms. The band structure results show that both phases are semiconductors (Figures 10A,B and 11A,B). The paraelectric phase is a direct band gap semiconductor with an energy gap of ∼0.66 eV at the Γ point and also has an indirect gap of the same size, ∼0.66 eV, with the valence band (VB) maximum along the H−A direction of the Brillouin zone (Figure 10B). The antiferroelectric phase is an indirect gap semiconductor with a much greater band-gap value of ∼1.1 eV (Figure 10A). The substantial increase in the gap is due to the restructuring of the top VB states, which are shifted down in energy. There is, however, a modification of all the VB states in going from the paraelectric to antiferroelectric phase (Figure 10B,A). The total energy comparison shows that the antiferroelectric phase lies lower in energy by ∼0.13 eV/fu than the paraelectric phase (fu = $CuBiP_2Se_6$). The VB maximum occurs along the Γ−L direction in the Brillouin zone of the antiferroelectric phase. This phase transition can be classified as a second-order Jahn−Teller distortion (see below).

To understand the atomic nature of the energy states, we can inspect the partial DOS. We find that the VB states between (−4.0 eV, 0 eV) have strong Cu d and Se p hybridized character (Figure 11C−F) and to a smaller degree Bi p and Se p hybridized character (Figure 11G,H). This suggests that there are strong covalent interactions between the Cu−Se and Bi−Se atoms, consistent with the chalcophilic nature of both metals. The paraelectric to antiferroelectric transition affects all the states (Cu d, Se p, and Bi p). Namely, the conduction band states in the range (1.0 eV, 5.0 eV) consist mostly of Bi p character with small contributions from P p character (Figure 11G,H). In the (−3.0 eV, 0 eV) energy interval, the Bi p states hybridize more extensively with the Se p states in the antiferroelectric phase than in the paraelectric phase.

The DOS plots suggest that the observed electronic optical absorption observed in the visible spectrum of $CuBiP_2Se_6$ (and by extension for $AgBiP_2Se_6$) is mainly due to excitations between filled Se-based p-orbitals and vacant Bi-based p-orbital states. The semiconducting energy gap is defined from the band maximum occurring along the Γ−L direction to the bottom of the unoccupied band at the Γ point (red arrow in Figure 10A). There is, however, another closely lying direct energy gap at the Γ point that is only slightly larger at ∼1.3 eV (blue arrow in Figure 10A). It is possible that the relatively sharp rise in optical absorption observed experimentally at ∼1.45 eV (Figure 1A) may involve both direct and indirect transitions, given these similarly spaced energy gaps. In fact, because the direct energy gap is expected to exhibit a greater absorption probability than the slightly smaller indirect gap, we may expect decent photoconductivity in these materials, and this conclusion is consistent with the previously reported results.[5]

Since experimentally we observe a phase transition from the para- to antiferroelectric state in the 298−97 K temperature interval, we wanted to check the relative stability of the antiferroelectric and hypothetical ferrielectric phases at 0 K. The ferrielectric phase which is not observed is defined by a model in which all Cu^+ ions in all layers move in the same direction along the *c*-axis, so that the same Cu−Se bond distances are achieved as in the antiferroelectric phase. Similarly, all Bi^{3+} ions in every layer are displaced in the opposite direction to the Cu^+ ions. We find that the total energy of the ferrielectric phase is higher by ∼0.19 eV/fu. This is consistent with the experimental results showing that the antiferroelectric phase is the ground state. Therefore, chemical bonding energetics dominate the Cu ion motion in $CuBiP_2Se_6$.

It is interesting to explore the driving force behind the off-center structural instabilities of Cu(Ag) and Bi^{3+} ions in these compounds. It is known that symmetry-breaking instabilities can occur as a result of a second-order Jahn−Teller d^{10}−s coupling between the conduction and valence band states.[25] Calculations carried out by Burdett et al.[26] and Wei et al.[27] for instabilities in the tetrahedral and octahedral symmetries support this idea. In the tetrahedral and octahedral

(24) During the stage of getting this manuscript in press, we discovered a brief report on $AgBiP_2S_6$. Seidlmayer, S.; Pfitzner, A. *Z. Anorg. Allg. Chem.* **2004**, *630*, 1759−1759.

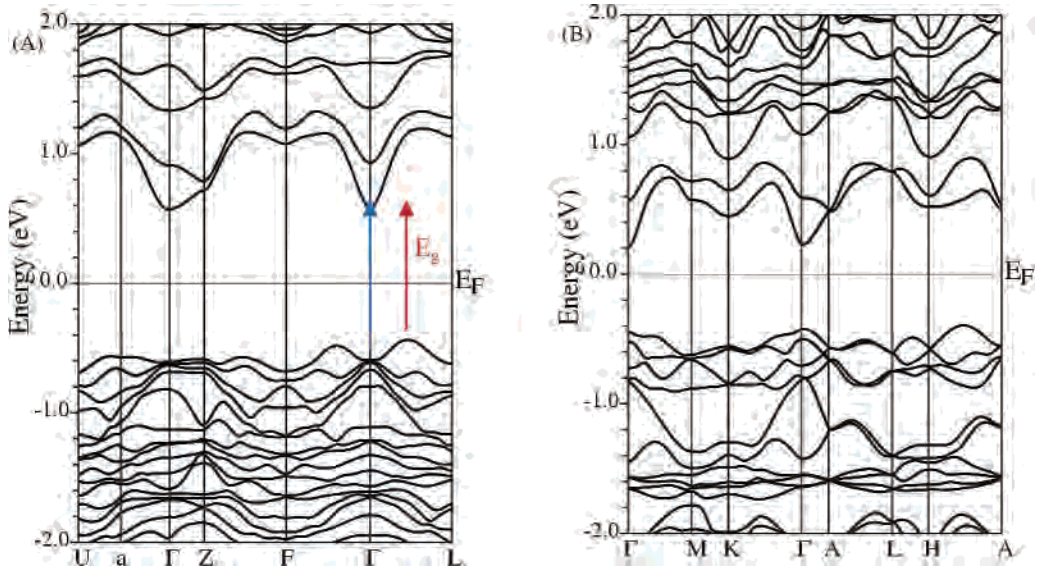

Figure 10. Band structure of $CuBiP_2Se_6$: (A) Antiferroelectric phase and (B) paraelectric phase.

symmetries the d−s mixing is not allowed. The mixing is allowed only if distortions from these symmetries occur and is accompanied by a lowering of energy. In contrast, in $CuBiP_2Se_6$, which has trigonal symmetry, the d−s mixing is allowed, even in the paraelectric (undistorted) phase (Figure 11J). The band calculation indicated only a small increase in the d−s mixing in the range (−1.5 eV, −0.5 eV) for the antiferroelectric phase (Figure 11I). More importantly, as can be seen from the DOS, the states responsible for the lowering in the energy of the antiferroelectric phase involve mostly d−p mixing, which is symmetry-allowed.

Consequently, a second-order Jahn−Teller effect associated with the d−p mixing is the driving force for the off-center displacement of Cu^+ (and Ag^+) ions in these compounds, which create three short Cu−Se2 bonds and three long Cu−Se1 bonds. The stabilization of the Se1 p orbitals is then achieved by shorter Se1−Bi bonds, due to the concomitant Bi displacement in the opposite direction to Cu(Ag). The displacement of the Bi atom in the opposite direction, which tends to cancel the intralayer dipole moment, is most likely assisted by the stereochemical expression of its $6s^2$ lone pair. The so-called lone pair could then occupy the space opposite to the direction of motion. Interestingly, in $CuInP_2Se_6$, which develops a ferroelectric phase, the lack of a lone pair in In^{3+} significantly reduces the ion's ability to shift in the opposite direction, which fails to cancel the incipient dipole moment created by the Cu^+ ions. The In^{3+} ion moves by only 0.2 Å, which is not adequate to cancel the much larger movement of 1.2 Å of the Cu^+ ions. This compares with a 0.3 Å shift for Bi^{3+} against a 3-fold opposite shift (1.16 Å) for Cu^+.

Although the above considerations explain well the driving force for intralayer ordering, they do not address the issue of why an interlayer antiferroelectric ordering of the dipole moments associated with the $Cu^+(Ag^+)$ and Bi^{3+} displacements is observed. It is clear that, due to the displacement of the $Cu^+(Ag^+)$ and Bi^{3+} ions in opposite directions, the net dipole moment inside a single $CuBiP_2Se_6$ slab is considerably reduced, but perhaps not minimized. This greatly reduces the dipole−dipole coupling between the layers, which in general favors an interlayer ferroelectric coupling.

To explore the origin of the antiferroelectric interlayer ordering (as seen in experiment), we have carried out crystal orbital Hamilton population (COHP)[28] analysis of the Se−Se interlayer bonds. COHP partitions the band structure states into bonding, nonbonding, and antibonding character, whereas the integrated COHP (ICOHP) gives the energy contribution of a bond to the total energy. We find that in the para and ferroelectric phases ICOHP is positive, decreasing the total energy (indicating antibonding character), whereas in the antiferroelectric phase ICOHP is small and negative, lowering the total energy. This suggests that the stability of the Se···Se interlayer van der Waals contacts may be responsible for the observed antiferroelectric ordering in these compounds.

Concluding Remarks

The coinage metal containing phases reported here are distinctly two-dimensional. Although the dimensionality is invariant upon switching from copper to silver, substantial differences exist between $CuBiP_2Se_6$ and $AgBiP_2Se_6$ with regard to the behavior of the two metals in their respective compounds. The coinage metal interaction with the anionic $[BiP_2Se_6]^{1-}$ framework is very strong relative to the corresponding alkali metal $ABiP_2Se_6$ analogues and in fact dominates the properties of the compounds. This includes a dramatic reduction in the energy gap and a tendency for

(25) Burdett, J. K. *Chemical Bonding in Solids;* Oxford University Press: Oxford, 1995, 24, 246.
(26) Burdett, J. K.; Eisenstein, O. *Inorg. Chem.* **1992**, *31*, 1758−1762.
(27) Wei, S. H.; Zhang, S. B.; Zunger, A. *Phys. Rev. Lett.* **1993**, *70*, 1639−1642.
(28) Dronskowshi, R.; Blochl, P. E. *J. Phys. Chem.* **1993**, *97*, 8617−8624.

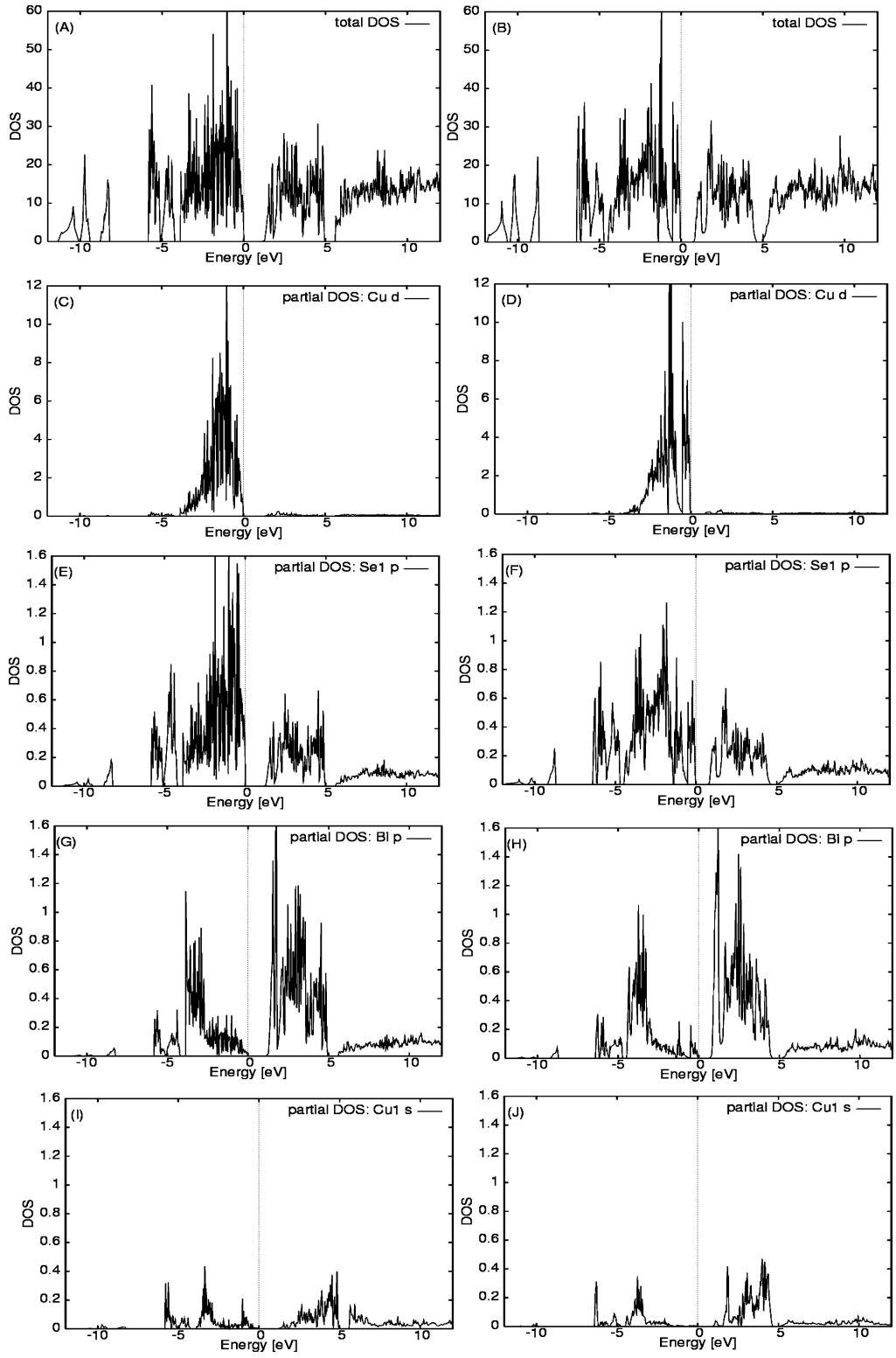

Figure 11. Total and partial atomic DOS: (A, C, E, G, I) antiferroelectric phase and (B, D, F, H, J) paraelectric phase.

structural distortion. The $[BiP_2Se_6]^{1-}$ framework adopts the lamellar $Fe_2P_2Se_6$ structure type motif, which is apparently stable enough to force the coinage metals, which tend to prefer lower coordination, into octahedral sites of Se atoms. In turn, the coordination preference of the coinage metal is satisfied by a motion toward one of the faces of the Se-based octahedron. The apparent tendency of the $[BiP_2Se_6]^{1-}$ framework to adopt the lamellar $Fe_2P_2Se_6$ structure type suggests that smaller alkali metals such as Na^+ and Li^+ may produce isostructural compounds to $CuBiP_2Se_6$ and $AgBiP_2Se_6$. A local dynamic hopping mechanism of Cu^+ ions is the basis for the antiferroelectric, second-order Jahn−Teller type instability that sets in with reduced thermal energy. A ferroelectric state in $CuBiP_2Se_6$ fails to develop, because of

counteracting opposite shifts in the Bi^{3+} ion sublattice. On the basis of this work, we conclude that in the lamellar system $CuMP_2Se_6$ (M = trivalent metal) several systems could exhibit ferroelectric or antiferroelectric phenomena, depending on the ability of M to undergo local motion. It would be interesting to explore whether motional frustration sets in due to competing interactions in mixed metal phases e.g. $CuIn_{1-x}Bi_xP_2Se_6$.

Acknowledgment. Financial support from the National Science Foundation (DMR-0443783) is gratefully acknowledged.

Supporting Information Available: Tables of crystallographic details, atomic coordinates, bond length and angles, and anisotropic thermal parameters for all compounds (CIF). This material is available free of charge via the Internet at http://pubs.acs.org.

IC050357+